Nanoscale

Accepted Manuscript

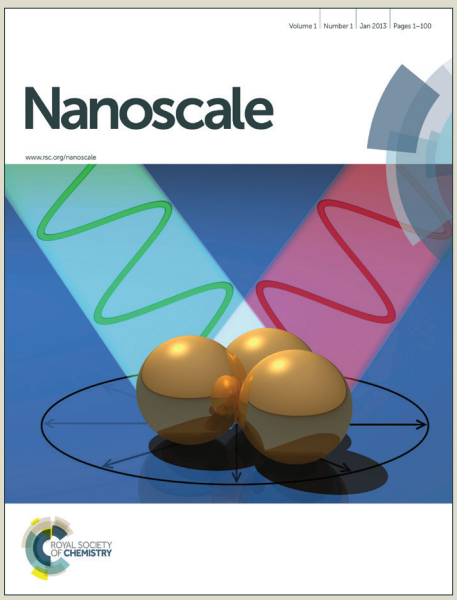

ROYAL SOCIETY OF CHEMISTRY

www.rsc.org/nanoscale

Nanoscale

ARTICLE

Received 00th January 20xx,
Accepted 00th January 20xx

DOI: 10.1039/x0xx00000x

www.rsc.org/

All-Optical Investigation of Tunable Picosecond Magnetization Dynamics in Ferromagnetic Nanostripes with Width Down to 50 nm

Susmita Saha[a], Saswati Barman[a], YoshiChika Otani[b,c], and Anjan Barman[a]*

Ferromagnetic nanostripes are important elements for a number of interesting technologies including magnetic racetrack memory, spin logic and magnonics. Understanding and controlling magnetization dynamics in such nanostripes are hence important problems in nanoscience and technology. Here we present an all-optical excitation and detection of ultrafast magnetization dynamics, including spin waves, in 5 μm long $Ni_{80}Fe_{20}$ nanostripes with varying stripe width from 200 nm down to 50 nm. We observed a strong width dependent variation in the frequency, anisotropy and spatial nature of spin waves in these systems. The effect of inter-stripe interaction is also studied and the 50 nm wide stripe is found to be nearly magnetostatically isolated, allowing us to detect the dynamics of a 50 nm wide individual stripe using an all-optical measurement technique. The tunability in magnetization dynamics with stripe width is important for their applications in various spin based technologies.

Introduction

Spin waves (SWs) are the fundamental magnetic excitations in a metallic ferromagnetic material having frequency in microwave regime similar to acoustic waves. The SW spectra in ferromagnetic materials with periodically modulated magnetic properties show allowed magnonic states with alternating forbidden band gaps. This forms a new class of artificial crystal known as magnonic crystal (MC)[1-3].They are magnetic counterpart of photonic and phononic crystals where SWs are used to transmit and process information. As the wavelengths of the SWs in gigahertz and sub-terahertz frequency regime are much shorter than those of light waves, magnonics is a more attractive technology for nanoscale on-chip microwave communication devices including magnonic

[a] Department of Condensed Matter Physics and Material Sciences, S. N. Bose National Centre for Basic Sciences, Block JD, Sector III, Salt Lake, Kolkata 700 098, India
[b] Institute for Solid State Physics, University of Tokyo, 5-1-5 Kashiwanoha, Kashiwa, Chiba 277-8581, Japan
[c] RIKEN-CEMS, 2-1 Hirosawa, Wako, Saitama 351-0198, Japan

*abarman@bose.res.in

waveguides[4], filters[5], splitters, phase shifters[6], as well as for magnonic logic devices[7].

Ordered arrays of magnetic nanostripes/nanowires have attracted considerable attention of the scientific community due to their intriguing physical properties as well as potential applications in microwave devices[8-9], data storage and domain wall logic[10]. They can beused as waveguides[4-5, 11] for SWs which is an important component of integrated magnonic circuits[12]. For unpatterened stripe dispersion curves for propagating dipole-exchange SWs are observed without any forbidden band. In contrary, allowed and forbidden bands are observed for stripes with periodically modulated width[13] and stripes with antidots[14].This make them one of the most promising candidates for one dimensional magnonic crystals (1D-MCs). Their large surface-to-volume ratio and inhomogeneous demagnetizing fields due to lateral confinement significantly influence their static and dynamic magnetic properties and hence, give rise to rich and complicated SW spectra in ferromagnetic stripes. The SWs in a ferromagnetic stripe can also be tuned through sample geometry[13, 15-16], propagation direction[17] and applied magnetic field[18-20]. In addition, ferromagnetic nanostripes/nanowires are important candidates for Racetrack Memory devices[21] mediated by controlled domain wall movement by current[22-23] or magnetic field[24]. In this regard the interaction of the domains with the intrinsic spin waves in such confined nanostructures would play an important role in the functionality of these devices. Hence, understanding of the SW dynamics in ferromagnetic nanostripes/nanowires is an important problem, which has not yet been studied in details.

Due to these interesting possibilities, the magnetization dynamics of micron and sub-micron wide longitudinally and transversely magnetized stripes have already been studied by various groups using Brillouin light scattering (BLS) experiment[16-17, 25-26], ferromagnetic resonance (FMR) experiment[19, 27] and time-resolved scanning Kerr microscopy (TRSKM)[28]. Interesting SW physics such as quantization[29], interference[30-31], filtering[8], and self-focusing[32]of SWs are observed in ferromagnetic nanostripes. The lateral quantization of the surface SWs due to the formation of lateral standing waves in a periodic array of micron sized stripes is already reported[21]. However, there are only few reports[28, 33] of picosecond magnetization dynamics of ferromagnetic stripes with micrometer sized width by using TRSKM. There, they observed the localized SW modes in backward volume (BV) and Damon-Eshbach (DE) geometries. However, picoseconds magnetization dynamics of ferromagnetic stripes with deep nanoscale dimensions have not been reported before. The possibility of tuning magnetization dynamics by varying the width of the stripe as well as the bias magnetic field orientation may lead towards interesting anisotropic magnetic properties suitable for applications in magnetic storage, memory, logic and communication devices. However, this has not been studied yet due to the difficulties in fabricating good quality high aspect ratio nanostripes with sub-100 nm width and the required thorough and non-trivial characterization.

In this present work we have overcome those difficulties. We fabricated high quality arrays of $Ni_{80}Fe_{20}$ (Py) nanostripes with width down to 50 nm and fixed length of 5 μm, and measured their time-resolved magnetization dynamics by varying the orientation of the bias magnetic field and the width of the stripe (from 50 to 200 nm). A remarkable variation in the spin wave quantization properties is observed with the variation of stripe width as well as the bias field orientation, which is modeled by using micromagnetic simulations. Finally, simulation of magnetostatic field distribution clearly shows that the 50 nm wide stripes are nearly magnetically isolated in the

array leading towards the measurement and understanding of magnetization dynamics of a single ferromagnetic nanostripe with 50 nm width.

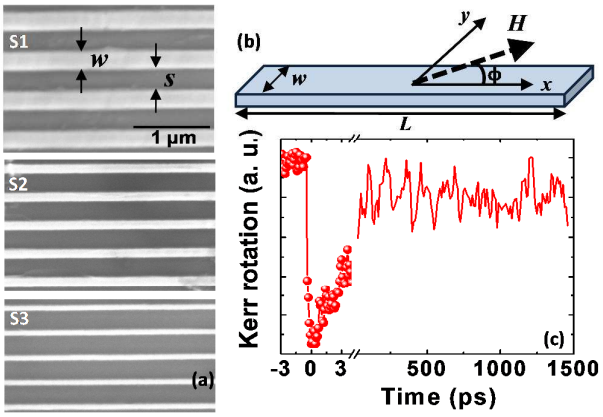

Figure 1. (a) Scanning electron micrographs of Py nanostripes with different stripe widths (S1, S2 and S3) are shown. (b) The schematic of the experimental configuration. Here, ϕ = 0° corresponds to backward volume (BV) geometry and ϕ = 90° corresponds to Damon-Eshbach (DE) geometry. (c) Typical experimental time-resolved Kerr rotation data from S3 (w = 50 nm) for H = 1 kOe applied at ϕ = 0°. The data reveals three different temporal regimes namely, the ultrafast demagnetization, fast and slow relaxations, and precession of magnetization.

Experimental Details

5 × 10 μm^2 arrays of 30 nm thick (t) and 5 μm long (L) Py nanostripes of width (w) 200 nm (S1), 100 nm (S2) and 50 nm (S3) were fabricated by a combination of electron beam lithography and electron beam evaporation technique. The edge to edge separation (s) of the stripes is fixed at a nominal value of 300 nm for all three samples to avoid strong dipolar interaction between the nanostripes. The scanning electron microscope (SEM) images of the nanostripes of different width are shown in **Figure 1(a)**. The SEM images show that the stripes are reasonably well prepared with slight deviations in the width and separation of the nanostripes from the nominal dimensions. The ultrafast magnetization dynamics of the samples are measured by using an all-optical time-resolved magneto-optical Kerr microscope[25-26] based upon two-color collinear pump-probe geometry. The second harmonic of a mode-locked Ti-sapphire laser is used to excite the magnetization dynamics in the samples whereas the time-delayed fundamental is used to probe the dynamics by measuring the Kerr rotation as a function of the time-delay between the pump and probe beams. The pump and probe beams are focused by using a single microscope objective (MO) nearly at the center (about 1 μm shifted from the centre along the length of the stripe) of the array of the nanostipes. This enabled us to capture all modes appeared at different positions along the length of the stripes. The pump beam excites the dynamics within a spot size of about 1 μm and the time delayed probe beam with spot size of 800 nm, placed at the center of the pump beam detect the magnetization dynamics by measuring the Kerr rotation as a function of the time delay between the pump and the probe beams. Between 2 and 3 nanostripes are probed during the measurements of three different samples. A bias field H = 1 kOe is applied to the sample, the direction of which was tilted slightly out of the plane of the sample to have a finite demagnetizing field along the direction of the pump pulse. The pump pulse rapidly modifies the out-of-plane demagnetizing field and thereby induces precessional magnetization dynamics within the dots. The azimuthal angle (ϕ) of the bias field H is varied between 0° and 90° at intervals of 15° by rotating the sample using a high precision rotary stage while keeping the microscope objective and the magnetic field constant. The schematic of the experimental geometry is shown in **Figure 1(b)**. The pump and the

probe beams are made to incident on the same nanostripes in the array after changing ϕ every time.

Figure 1(c) shows a typical time-resolved Kerr rotation data from the nanostripe with 50 nm width at H = 1 kOe applied at $\phi = 0^{\circ}$. The data shows an ultrafast demagnetization within 500 fs of the zero delay and subsequent bi-exponential remagnetization with time constants of 3.3 ps and 84 ps. The faster relaxation occurs because the hot electrons and the spins exchange energy with the lattice via electron–phonon interaction whereas the slower relaxation corresponds to the transfer of energy to the substrate and the surrounding[34]. The precessional dynamics appears as an oscillatory signal on top of the slowly decaying time-resolved Kerr rotation. The negative time-delay and the ultrafast demagnetization signal is eliminated and a bi-exponential background corresponding to the two step relaxation is subtracted from the time-resolved data before performing a fast Fourier transform (FFT) on the data. A total time-delay of about 1.5 ns at time steps of 5 ps is used for the FFT analysis.

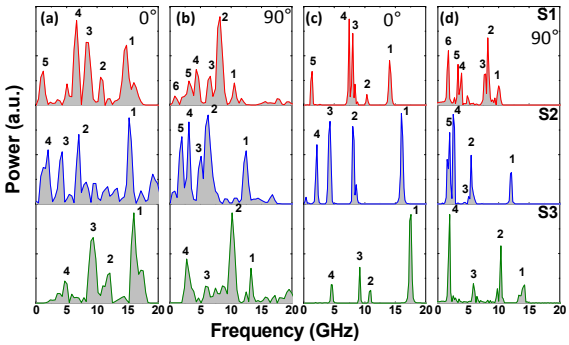

Figure 2. Experimental SW spectra at (a) ϕ = 0°, (b) ϕ = 90° and simulated SW spectra at (c) ϕ = 0°, (d) ϕ = 90° are shown for S1, S2 and S3 at H = 1.0 kOe.

Result and Discussions

Figures 2(a) and **(b)** show experimental SW spectra of S1, S2 and S3 for bias field H = 1 kOe applied at $\phi = 0^{\circ}$ and 90°, respectively. A clear variation in the SW spectra is observed for different samples and also with the orientation of the bias field. In all cases rich SW spectra with a number of modes are observed. While for $\phi = 0^{\circ}$, the modes span upto about 17 GHz, the bandwidth is little less (about 14 GHz) for $\phi = 90^{\circ}$. At $\phi = 0^{\circ}$ five modes are observed in S1, whereas the number of modes reduces to four for S2 and S3. The frequency of mode 1 increases with the decrease of the width of the stripe (increase in aspect ratio L/w) and it attains a maximum value in S3 having an aspect ratio of 100. In our measurement the ratio length/width/thickness ($l/w/t$) is varied from 5000/50/30 to 5000/200/30. The demagnetization factor along the nanostripe length can be expressed as $N_l \sim 2t/\pi l$ while the same along the nanostripe width is $N_w \sim 2t/\pi w$[35]. The shape anisotropy field (H_{sh}) is proportional to the difference in the demagnetization fields in two orthogonal directions which can be expressed as $H_{sh} = M_s(N_l - N_w) \sim (2t/\pi w)(w/l - 1)$. In our case $w/l \ll 1$, and as a result H_{sh} can be approximated as $2t/\pi w$ i.e., inversely proportional to the width of the stripe. Consequently, the shape anisotropy will increase with the decrease in stripe width.

At $\phi = 90^{\circ}$ six modes are observed for S1and the number of modes gradually reduces to five and four for S2 and S3, respectively. In addition, the frequencies of all modes for all three samples are decreased significantly for $\phi = 90^{\circ}$ as opposed to those for $\phi = 0^{\circ}$. This is due to the reduction in the effective magnetic field along the bias field direction for $\phi = 90^{\circ}$. However, the detailed spin configuration of the magnetic ground states for different samples at different orientations of the bias magnetic field would play crucial role in determining the details of the SW spectra.

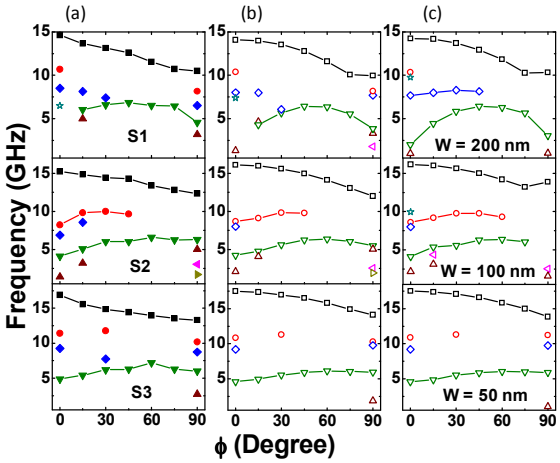

Figure 3. (a) Experimental (filled symbols) and (b) simulated SW frequencies (open symbols) as a function of the azimuthal angle ϕ of the in-plane bias magnetic field at H =1 kOe for S1, S2 and S3. (c) Simulated SW frequencies (symbols) as a function of the azimuthal angle ϕ of the in-plane bias magnetic field at H = 1 kOe for single nanostripes of widths w = 200 nm, 100 nm and 50 nm. The solid lines are only connecting the experimental and simulated SW frequencies.

Subsequently, we measured the magnetization dynamics as a function of ϕ at a fixed strength of H = 1 kOe. The variation of all the experimentally observed peak frequencies with ϕ is plotted in **Figure 3(a)**. It is observed from Figure 3(a) that a number of modes at $\phi = 0^{\circ}$ for all samples converge into two modes at around $\phi = 60^{\circ}$ and again diverge to the same number of modes at $\phi = 90^{\circ}$. All the SW modes show anisotropic behavior but it is difficult to fit the variation of the precessional frequency by using modified Kittel formula for reason that will be discussed later in this manuscript.

Micromagnetic simulations were performed considering arrays consisting of three stripes using OOMMF[36] software to reproduce the experimental results. To understand the role of inter-stripe interaction further test simulations considering five stripes were also performed, which shows a variation in the relative intensities but the number and frequencies of the SW modes remain unchanged and hence for optimizing computational resources we performed simulations with three stripes in this manuscript. The samples were discretized into rectangular prism-like cells with dimensions 5 × 5 × 30 nm^3. The lateral cell size is below the exchange length (5.3 nm) of Py. The absence of discretization along the stripe thickness is justified as we did not observe any perpendicular standing spin waves in these stripes. The parameters used for the simulation are γ = 17.6 MHz/Oe, exchange stiffness constant, $A = 1.3\times10^{-6}$ erg/cm, magnetocrystalline anisotropy constant K = 0 and saturation magnetization M_s = 860 emu/cc. The external bias field is applied according to the experimental configuration and a pulsed field of rise time of 50 ps and peak amplitude of 30 Oe is applied perpendicular to the sample plane. **Figures 2(c, d)** show the FFT power spectra of the simulated time-domain magnetization for all three samples at $\phi = 0^{\circ}$ and 90°, respectively. The simulated results qualitatively reproduced the experimental observations. The relative intensities and the precise positions of the peaks in the frequency domains are not always quantitatively reproduced because of lack of inclusion of the precise edge roughness and other defects in the simulated samples as observed experimentally. In addition, the optical excitation is replaced by pulsed magnetic field in the simulation. **Figure 3(b)** shows the variation of the simulated precessional frequency for different samples with the azimuthal angle (ϕ) of the bias field. The important features including the rich and broad SW spectrum, the number of SW modes and their variation with the azimuthal angle (ϕ) of the bias magnetic field are well reproduced using micromagnetic simulations.

We have also simulated the magnetization dynamics of single nanostripes of different widths to understand the intrinsic modes of the single stripes and how they got affected by the other stripes when placed in an array. **Figure 3(c)** shows the variation of the simulated mode frequencies with the azimuthal angle (ϕ) of the bias field for single stripes of different widths. For the wider stripes (S1 and S2) there is a sharp difference in the number of modes between single stripe and arrays of stripes whereas it remains identical for the narrowest stripe S3. This indicates that while S1 and S2 are significantly influenced by the inter-stripe interaction, the nanostripes in S3 are nearly magnetically isolated.

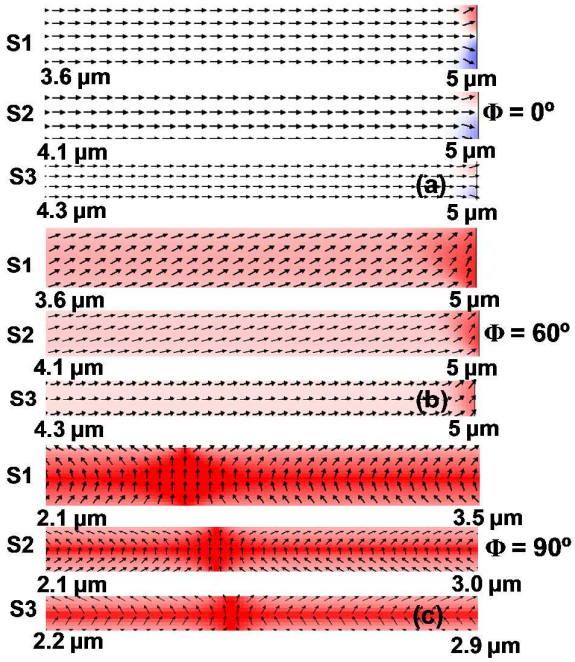

Figure 4. Simulated static magnetic configurations for S1, S2 and S3 are shown for H = 1 kOe applied at (a) ϕ = 0°, (b) ϕ = 60° and (c) ϕ = 90°. The region close to right edge of the stripe is shown in (a) and (b), whereas the center of the stripe is shown in (c). The y-component of magnetization vector is represented by blue-white-red color map. The horizontal lengthscale is shown below each stripe for convenience.

Figures 4(a, b, c) show the static magnetic configurations of the central stripe from the simulated arrays corresponding to S1, S2 and S3 for ϕ = 0°, 60° and 90°. For each stripe the static magnetic image from the centre to the right edge of the stripe is shown for convenience. At ϕ = 0° all three stripes show uniform magnetization parallel to the bias field with a small flower like state near the stripe ends. At ϕ = 60° all three stripes show leaf like state. However, only for S1 the magnetization is nearly parallel to the bias field and it started to deviate towards the long axis of the stripe with decreasing stripe width and the deviation is maximum for S3. At ϕ = 90°, a completely different magnetic state is observed in all three samples where two domains with clock-wise and anticlock-wise C-states separated by a transverse domain wall is observed. In addition, for S1 and S2, the spins near the axis of the stripes are parallel to the bias field while the spins towards the two edges systematically deviate from the bias field direction. This allows us to divide the stripes (waveguides) in two sub-waveguides. However, this is not possible for S3 as all spins are deviated from the bias field in this case.

Nanoscale

ARTICLE

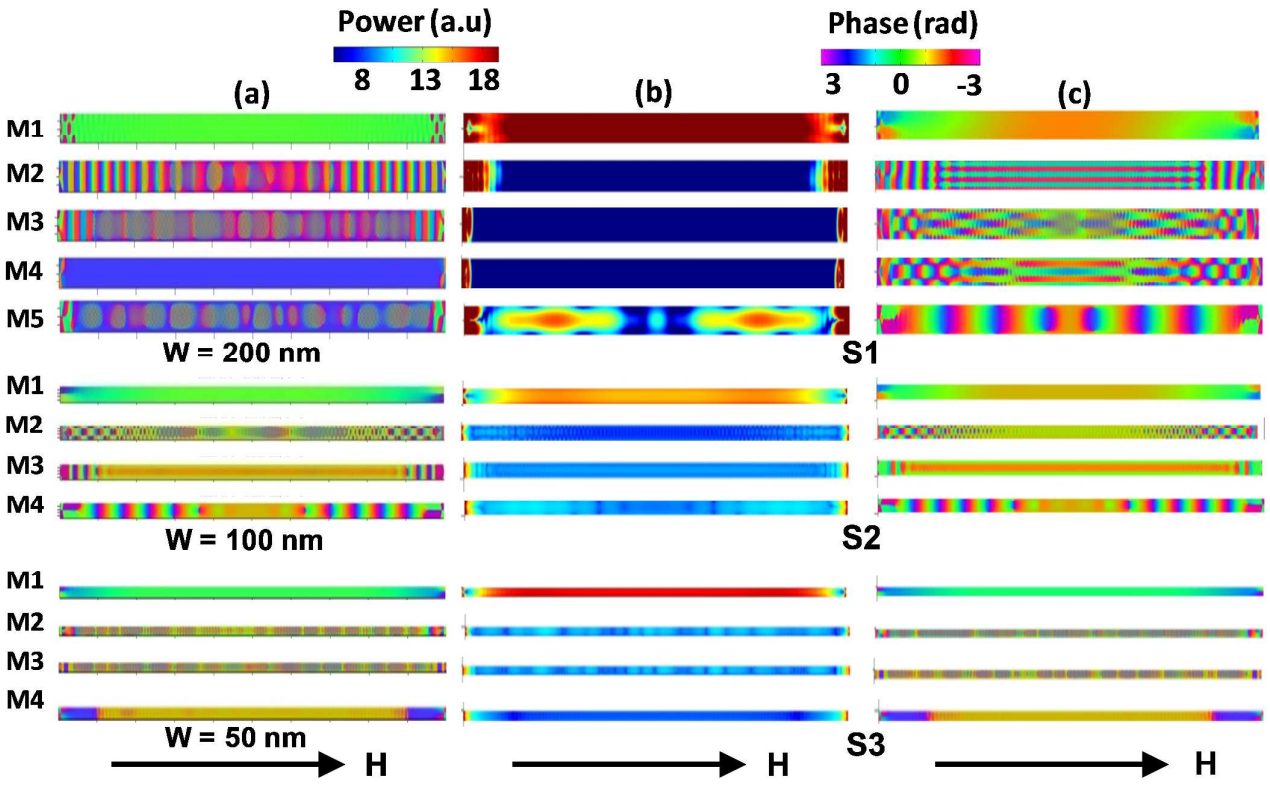

Figure 5. (a) The phase profiles of all SW modes for single stripes of three different widths for H = 1 kOe applied at ϕ = 0°. The (b) power and (c) phase profiles of all simulated SW modes for S1, S2 and S3 for H = 1 kOe applied at ϕ = 0°. The color maps for power and phase distributions are shown at the top of the figure. The direction of external bias magnetic field (H) is shown at the bottom of the figure. The widths of all stripes are increased by a factor of two for clear visualization of the quantized SW modes.

For further understanding, we numerically calculated the SW mode profiles of single stripes and arrays of stripes using a home build code[37]. **Figure 5(a)** shows the phase maps of SW mode profiles of single stripes of width 200, 100 and 50 nm at $\phi = 0^{\circ}$. It is clear from Figure 5(a) that at $\phi = 0^{\circ}$, the 200 nm and 50 nm wide single stripes show standing SWs in backward volume (BV) geometry, whereas for the stripe with intermediate width (w = 100 nm), standing SWs with a combination of Damon-Eshbach (DE) and BV geometry are observed. However, the modes are significantly modified for the wider stripes (w = 200 nm and 100 nm) when they are arranged in

an array (S1 and S2). In Figures 5(b and c) the power and phase profiles of the resonant modes for S1, S2 and S3 are shown. From **Figure 5(b, c)** it is observed that mode 1 (M1) for S1 and S2 correspond to the uniform precessional mode at the centre of the

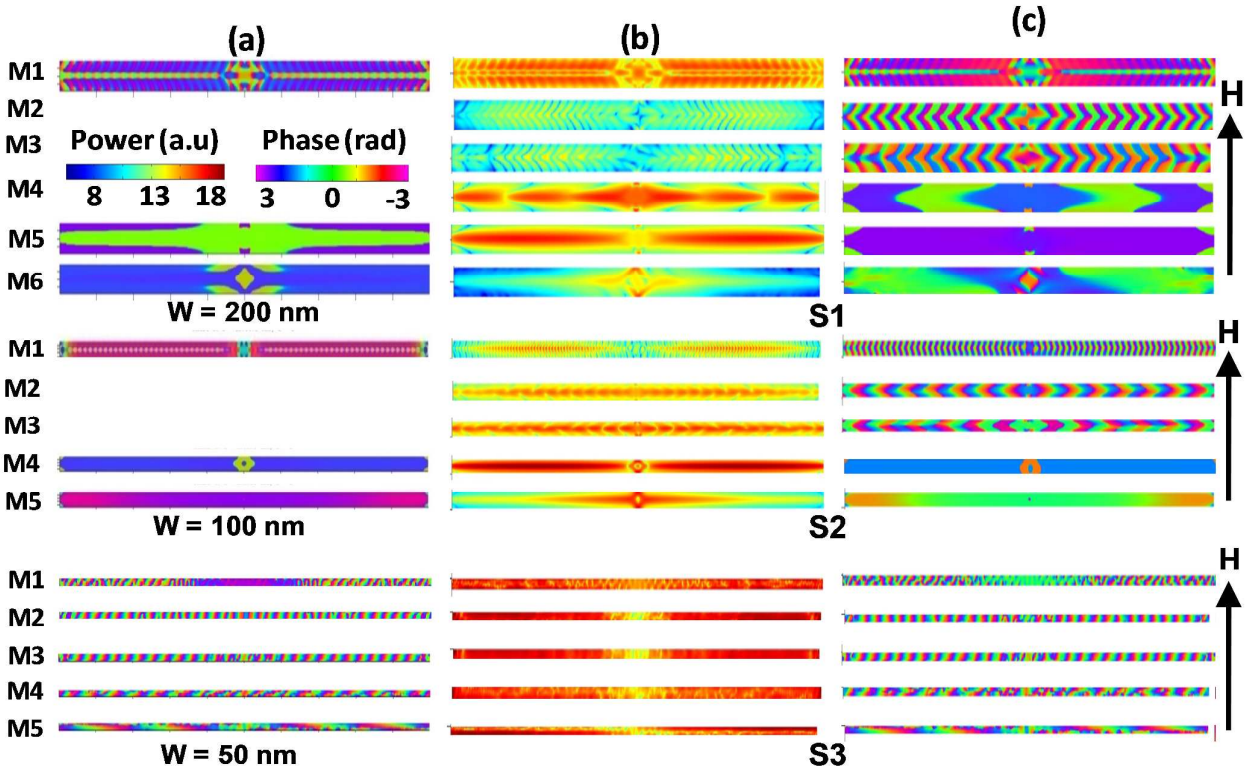

Figure 6. (a) The phase profile of all SW modes for single stripes of different widths for H = 1 kOe applied at ϕ = 90° are shown. The (b) power and (c) phase profiles of all SW modes for S1, S2 and S3 for H = 1 kOe applied at ϕ = 90° are shown. The color maps for power and phase distributions are shown in (a). The direction of external bias magnetic field (H) is shown at the right of the figure. The widths of all stripes are increased by a factor of two for clear visualization of the quantized SW modes.

stripe (centre mode). However, M2, M3, M4 for S1 and M2, M3 for S2 are quantized modes with combination of DE and BV geometries. While the standing SWs of BV (mode quantization number: n) geometry are primarily confined near the stripe edges, the DE-like modes (mode quantization number: m) are located near the centre of the stripe. The quantization numbers m of the DE modes for M2, M3 and M4 for S1 are 5, 3 and 3, respectively whereas for M2 and M3 in S2, m = 3 for both modes. The quantization number n for the BV-like standing SW modes could not be determined due to the lack of resolution of this mode for most parts of the stripe. In contrary to the other modes, M5 for S1 and M4 for S2 are both BV-like standing SW modes with quantization number (n) 15 and 29, respectively. On the other hand, the mode structure in S3 is completely different than S1 and S2. Further for this sample the modes are identical to those of a single stripe of same width. Here, M1 is the centre mode whereas M2, M3 and M4 are all BV-like standing SW modes but the mode numbers could not be counted due to the lack of spatial resolution.

Nanoscale

ARTICLE

The phase profile of single nanostripes with three different widths at ϕ = 90° are shown in **Figure 6(a)**. For wider stripes (w = 200 and 100 nm) three modes each are observed in single stripes, while for the arrays of those the number of modes changed to 6 (S1) and 5(S2). Further, for the stripe with w = 200 nm, only mode 1 retained its identity in the array while the other two modes disappeared in the array. In contrary, for the stripe with w = 100 nm all three modes retained their identities in the array. The demagnetized region right on the long axis of the stripe divided the stripe into two sub-stripes and modes in the lower sub-stripe are mirror images of those in the upper sub-stripe. In addition, the quantization axes of the standing SW modes deviate substantially from the long axis of the stripe creating arrow-like standing SW modes (Modes M1 to M4 for S1 and modes M1 to M3 for S3). As shown in **Figure 6(b, c)** M1, M2, M3, M4 for S1and M1, M2, M3 for S2 are arrow-like standing SW modes with quantization number (n) 69, 45, 41, 5 for S1 and 121, 29, 25 for S2, respectively. M5 for S1 and M4 for S2 correspond to uniform (centre) modes, while M6 for S1 and M5 for S2 are DE-like standing SW modes with n = 3. As for ϕ = 90°, in S3 the modes are again identical to the modes observed for the single stripe. Here, all modes correspond to DE-like standing SW modes with their quantization axes deviated from the direction of the long-axis of the stripe. While the mode quantization number n could not be counted for M1 due to lack of resolution, the values of n are observed as 61, 57, 37 and 11 for M2, M3, M4 and M5, respectively. From the simulated mode profiles, it is observed that for all three samples standing SW is formed either in BV-like geometry or in DE-like (arrow-like) geometry with different quantization numbers depending upon the orientation of bias magnetic field (ϕ). As a result it is not appropriate to model the anisotropy of the spin wave frequency with the orientation of the bias magnetic field using a modified Kittel formula because it is only valid for uniform precessional mode (Kittel mode).

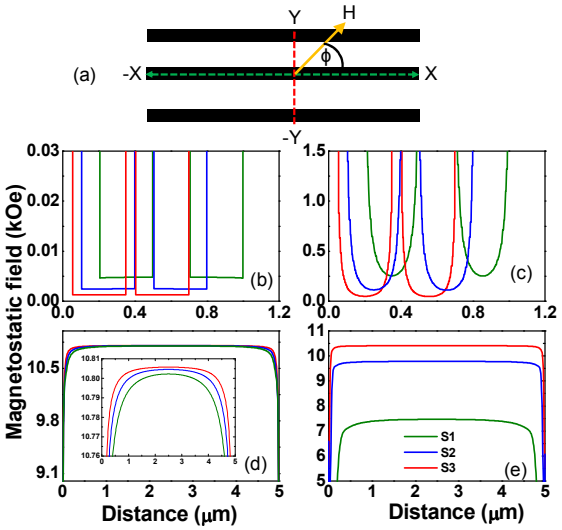

Figure 7. (a) The schematic of the linescan of the simulated magentostatic field and the geometry of the applied magnetic field for the array of stripes are shown. The linescans of the simulated magnetostatic fields ($(B = B_x^2 + B_y^2)^{1/2}$) along Y (red dotted line) direction from S1, S2 and S3 for H = 1 kOe applied at (b) $\phi = 0^{\circ}$ and (c) $\phi \approx 90^{\circ}$ are shown. The linescans of the simulated magnetostatic fields along X direction (X-component) (green dotted line) from S1,

S2 and S3 for H = 1 kOe applied at (d) $\phi = 0^{\circ}$ and (e) $\phi \approx 90^{\circ}$ are shown.

To understand the collective behavior of the magnetization dynamics, we have simulated the magnetostatic field distributions in the arrays of nanostripes. For all three samples at ϕ = 0°, the spins are fully aligned parallel to the boundaries of the stripes leaving no free magnetic charges at the stripe boundaries. As a result the inter-stripe interaction is negligible as shown by linescans of magentostatic field (**Figure 7(b)**) along the red dashed line in **Figure 7(a)**. However, at ϕ = 90°, the spins deviate from being parallel to the long boundaries of the stripes creating some free magnetic charges at those boundaries and consequently finite amounts of inter-stripe interaction fields. From **Figure 7(c)** it is observed that the inter-stripe interaction is maximum (261 Oe) for S1 and minimum (52 Oe) for S3 and has an intermediate (118 Oe) value for S2. We have further calculated the linescans of the magnetostatic fields along the length of the central stripes (green dashed line) from the three arrays for $\phi = 0^{\circ}$ and $\phi \sim 90^{\circ}$ as shown in **Figures 7(d, e)**. At $\phi = 0^{\circ}$, the internal field is uniform at about 10.8 kOe for 80% of the stripe length barring the edge regions, where the field curves off from the flat line with highest curvature for S1, which decreases with increasing aspect ratio. The inset clearly shows a small difference in the internal field between three samples. At $\phi \sim 90^{\circ}$, the spin configurations for three different stripes are very different leading to a large difference in the internal field, spin wave frequencies and mode structures as well. Figure 7(e) confirms that the shape anisotropy is maximum for S3 and minimum for S1 and the shape anisotropy of the stripe increases as the aspect ratio of the stripe increases.

Conclusions

In conclusion, we have investigated the ultrafast magnetization dynamics of $Ni_{80}Fe_{20}$ nanostripes of three different widths by varying the orientation of the external bias magnetic field using all-optical time-resolved magneto-optical Kerr microscopy. For the narrowest stripe with 50 nm width the inter-stripe interaction becomes negligible enabling us to detect the dynamics of a single 50 nm wide stripe. We have observed a significant difference in the spin wave frequencies and nature of modes with the variation of the width of the stripe as well as by varying the bias field orientation. When the bias field is applied along the length of the stripes the wider stripes (w = 200 and 100 nm) showed uniform mode, a combination of BV- and DE-like standing spin wave modes and pure BV-like standing spin wave mode. However the 50 nm wide stripe showed only uniform mode and pure BV-like standing spin waves. As the bias field is rotated towards the stripe width the 200 and 100 nm wide stripes showed arrow-like standing spin waves, while for the 50 nm wide stripe only DE-like standing spin waves with quantization axis deviated from the stripe axis is observed. Simulated magnetostatic field distribution gives further evidence for the variation of the spin waves with stripe width and bias field orientation and confirmed a single stripe like behavior for the 50 nm wide stripe. The width dependent quantization of SWs in magnetic stripes opens up opportunities in engineering of domain-wall, spintronic and magnonic devices.

Acknowledgements

We acknowledge the financial assistance from Department of Science and Technology, Govt. of India under grant no. SR/NM/NS-09/2011 and SR/NM/NS-53/2010, and S. N.Bose National Centre for Basic Sciences for the grant SNB/AB/12-

13/96. S. S. acknowledges UGC, Government of India for the senior research fellowship. We also thank T. Aoki and Dheeraj Kumar for technical assistances during this work.

Notes and references

Fabrication: Rectangular arrays of Py stripes were fabricated using a combination of electron beam lithography and electron beam evaporation techniques. Patterned structures were prepared on self oxidized Si (100) substrate coated by MMA/PMMA (Methyl Methacrylate/Polymethyl Methacrylate) resist with a beam current 100 pA for a dose time of 1.0 µs. After developing the resist pattern Py was deposited using electron beam evaporation at a base pressure of about 2×10^{-8} Torr. A 5 nm thick Al_2O_3 layer is deposited on top of the Py layer to protect it from degradation when exposed in the environment as well as to high fluence femtosecond lasers during the measurement. This is followed by the lifting off of the sacrificial material and oxygen plasma cleaning of the residual resists that remained even after the lift-off process.

Measurement: The ultrafast magnetization dynamics of the arrays of nanostripes was measured by using a home-built time-resolved magneto-optical Kerr microscope which is based upon femtosecond two colour pump-probe technique. The setup is based upon a mode locked Ti-sapphire pulsed laser source (Tsunami, Spectra physics) with tunable wavelength between 700 and 1000 nm and pulse-width of about 80 fs. The second harmonic (λ_B = 400 nm, fluence ≈ 16 mJ/cm^2, pulsewidth ≈ 100 fs) of the fundamental laser is used to excite the magnetization dynamics of the sample. The plane polarized fundamental laser beam (λ_R = 800 nm, fluence ≈ 3 mJ/cm^2) is used to probe the magnetization dynamics after passing through a variable time delay by measuring the change in the polar Kerr rotation of the reflected probe beam by an optical bridge detector in a phase-sensitive manner. The pulsewidth of the fundamental laser is measured by using an autocorrelator (model number: A•P•E Pulse Check USB). The pump and probe beams are made collinear and are focused slightly away (~1 µm) from the centre along the length of the stripe of the each sample through a microscope objective with N.A. = 0.65. The sample is placed on a piezoelectric scanning X-Y-Z stage with a feedback loop for better stability. At the focal plane of the probe (diameter ≈ 800 nm), i.e., on the sample surface, the pump beam is slightly defocused, and has a larger diameter (≈ 1µm) than the probe beam, which makes it easier to overlap the pump and probe beams on the sample surface. The two-color collinear pump-probe geometry enables us to achieve a very good spatio-temporal resolution and detection sensitivity in our measurements. An external magnetic field (H) is applied at a small angle (10°) to the sample plane to create an out-of-plane component of the bias field which creates a finite demagnetizing field within the sample along the direction of the pump pulse. This field is modified by the pump pulse to induce a precessional motion of magnetization within the samples. The pump beam was chopped at a frequency of 2 kHz and a phase sensitive detection of total reflectivity and Kerr rotation signals are measured with the help of two lock-in amplifiers.

Numerical Simulation: We have performed micromagnetic simulations at T = 0 K using the OOMMF software to obtain the SW spectra for different samples. The samples are divided into rectangular prism-like cells with dimensions $5 \times 5 \times 30$ nm^3. The lateral dimensions of the cells are less than the exchange length (5.3 nm) of Py and hence exchange interaction field is included in the simulation. The static magnetic configuration is achieved by

applying a large magnetic field (+10 kOe) sufficient to saturate the magnetization of the sample followed by reduction of the magnetic field to the designated bias field value and the system is allowed to relax for a long enough time to achieve the equilibrium state (maximum torque $\boldsymbol{m} \times \boldsymbol{H}$ where $\boldsymbol{m} = \boldsymbol{M}/M_S$, goes well below 10^{-6} A/m). The dynamics was simulated by applying a pulsed magnetic field of 50 ps rise time and 30 Oe peak value, and by calculating the spatial distribution of magnetization at time steps of 10 ps for a total duration of 4 ns. The convergence criterion for the dynamical calculation is set on the time steps. The spatial maps of the power and phase information for various SW modes are obtained by fixing one of the spatial co-ordinates in the space and time dependent magnetization followed by performing a discrete Fourier transform with respect to time domain.

1. V. V. Kruglyak, S. O. Demokritov and D. Grundler, *J. Phys. D: Appl. Phys.,***2010**, *43*, 264001.

2. S. Neusser and D. Grundler, *Adv. Mater. ,***2009**, *21*, 2927.

3. B. Lenk, H. Ulrichs, F. Garbs and M. Münzenberg, *Phys. Rep.,***2011**, *507*, 107.

4. J. W. Kłos, D. Kumar, J. Romero-Vivas, H. Fangohr, M. Franchin, M. Krawczyk and A. Barman, *Phys. Rev. B,***2012**, *86*, 184433.

5. S.-K. Kim, K.-S. Lee and D.-S. Han, *Appl. Phys. Lett.,***2009**, *95*, 082507.

6. Y. Au, M. Dvornik, O. Dmytriiev and V. V. Kruglyak, *Appl. Phys. Lett.,***2012**, *100*, 172408.

7. D. A. Allwood, G. Xiong, C. C. Faulkner, D. Atkinson, D. Petit and R. P. Cowburn, *Science,***2005**, *309*, 1688.

8. S. Choi, K.-S. Lee, K. Y. Guslienko and S.-K. Kim, *Phys. Rev. Lett.,***2007**, *98*, 087205.

9. S. Zhang, S. A. Oliver, N. E. Israeloff and C. Vittoria, *Appl. Phys. Lett. ,***1997**, *70*, 2756.

10. X. Zhu, D. A. Allwood, G. Xiong, R. P. Cowburn and P. Grütter, *Appl. Phys. Lett.,***2005**, *87*, 062503.

11. J. W. Kłos, D. Kumar, M. Krawczyk and A. Barman, *Sci. Rep.,***2013**, *3*, 2444.

12. S.Urazhdin, V.E.Demidov, H.Ulrichs, T.Kendziorczyk, T.Kuhn, J.Leuthold, G.Wilde and S.O.Demokritov, *Nat Nano,***2014**, *9*, 509.

13. K.-S. Lee, D.-S. Han and S.-K. Kim, *Phys. Rev. Lett.,***2009**, *102*, 127202.

14. D. Kumar, P. Sabareesan, W. Wang, H. Fangohr and A. Barman, *J. Appl. Phys.,***2013**, *114*, 023910.

15. G. Gubbiotti, S. Tacchi, G. Carlotti, P. Vavassori, N. Singh, S. Goolaup, A. O. Adeyeye, A. Stashkevich and M. Kostylev, *Phys. Rev. B,***2005**, *72*, 224413.

16. M. P. Kostylev, G. Gubbiotti, J. G. Hu, G. Carlotti, T. Ono and R. L. Stamps, *Phys. Rev. B,***2007**, *76*, 054422.

17. J. Topp, J. Podbielski, D. Heitmann and D. Grundler, *Phys. Rev. B,***2008**, *78*, 024431.

18. J. Ding, M. Kostylev and A. O. Adeyeye, *Phys. Rev. Lett.,***2011**, *107*, 047205.

19. C. Schoeppner, K. Wagner, S. Stienen, R. Meckenstock, M. Farle, R. Narkowicz, D. Suter and J. Lindner, *J. Appl. Phys.,***2014**, *116*, 033913.

20. S. Parkin and S.-H. Yang, *Nat Nano,***2015**, *10*, 195.

21. I. M. Miron, T. Moore, H. Szambolics, L. D. Buda-Prejbeanu, S. Auffret, B. Rodmacq, S. Pizzini, J. Vogel, M. Bonfim, A. Schuhl and G. Gaudin, *Nat Mater,***2011**, *10*, 419.

22. S.-H. Yang, K.-S. Ryu and S. Parkin, *Nat Nano,***2015**, *10*, 221.

23. G. S. D. Beach, C. Nistor, C. Knutson, M. Tsoi and J. L. Erskine, *Nat Mater,***2005**, *4*, 741.

24. J. Jorzick, S. O. Demokritov, B. Hillebrands, M. Bailleul, C. Fermon, K. Y. Guslienko, A. N. Slavin, D. V. Berkov and N. L. Gorn, *Phys. Rev. Lett.,***2002**, *88*, 047204.

25. M. Kostylev, P. Schrader, R. L. Stamps, G. Gubbiotti, G. Carlotti, A. O. Adeyeye, S. Goolaup and N. Singh, *Appl. Phys. Lett.,***2008**, *92*, 132504.

26. K. L. Livesey, J. Ding, N. R. Anderson, R. E. Camley, A. O. Adeyeye, M. P. Kostylev and S. Samarin, *Phys. Rev. B,***2013**, *87*, 064424.

27. J. P. Park, P. Eames, D. M. Engebretson, J. Berezovsky and P. A. Crowell, *Phys. Rev. Lett.,***2002**, *89*, 277201.

28. C. Mathieu, J. Jorzick, A. Frank, S. O. Demokritov, A. N. Slavin, B. Hillebrands, B. Bartenlian, C. Chappert, D. Decanini, F. Rousseaux and E. Cambril, *Phys. Rev. Lett.,***1998**, *81*, 3968-3971.

29. R. Hertel, W. Wulfhekel and J. Kirschner, *Phys. Rev. Lett.,***2004**, *93*, 257202.

30. J. Podbielski, F. Giesen and D. Grundler, *Phys. Rev. Lett.,***2006**, *96*, 167207.

31. V. E. Demidov, S. O. Demokritov, K. Rott, P. Krzysteczko and G. Reiss, *Phys. Rev. B,***2008**, *77*, 064406.

32. O. Dmytriiev, U. A. S. Al-Jarah, P. Gangmei, V. V. Kruglyak, R. J. Hicken, B. K. Mahato, B. Rana, M. Agrawal, A. Barman, M. Mátéfi-Tempfli, L. Piraux and S. Mátéfi-Tempfli, *Phys. Rev. B,***2013**, *87*, 174429.

33. V. V. Kruglyak, P. S. Keatley, A. Neudert, M. Delchini, R. J. Hicken, J. R. Childress and J. A. Katine, *Phys. Rev. B,***2008**, *77*, 172407.

34. A. Laraoui, J. Vénuat, V. Halté, M. Albrecht, E. Beaurepaire and J.-Y. Bigot, *J. Appl. Phys.,***2007**, *101*, 09C105.

35. Y. P. Ivanov, O. Iglesias-Freire, E. V. Pustovalov, O. Chubykalo-Fesenko and A. Asenjo, *Phys. Rev. B,***2013**, *87*, 184410.

36. M. Donahue and D. G. Porter, *OOMMF User's guide, Version 1.0,*. (NIST Interagency Report No. 6376,National Institute of Standard and Technology, Gaithersburg, MD, URL: http://math.nist.gov/oommf, 1999).

37. D. Kumar, O. Dmytriiev, S. Ponraj and A. Barman, *J. Phys. D: Appl. Phys.,***2012**, *45*, 015001.

Table of Content

We present the time domain investigation of optically induced ultrafast magnetization dynamics in arrays of $Ni_{80}Fe_{20}$ nanostripes of three different widths (w) of 50, 100 and 200 nm. Rich magnetization dynamics showing an ultrafast demagnetization, relaxation and generation of spin waves (SWs) with frequencies spreading between 2 to 17 GHz are observed. A strong width dependent variation in the frequency, anisotropy and spatial nature of spin waves indicates application of these nanostripes in tunable spintronic and magnonic devices. The 50 nm wide stripe show negligible inter-stripe interaction enabling us to detect a single nanostripe dynamics down to 50 nm lengthscale.

Keyword Magnetic Nanostripes, Ultrafast Magnetization Dynamics, Time-resolved Magneto-optical Kerr Microscopy, Spin Waves